LASER INTERFEROMETER GRAVITATIONAL WAVE OBSERVATORY
- LIGO -
CALIFORNIA INSTITUTE OF TECHNOLOGY
MASSACHUSETTS INSTITUTE OF TECHNOLOGY

Technical Note **LIGO-T1300786-v6** Date:10/26/2013

LIGO III Quad Pendulum Conceptual Design Optimization

Brett Shapiro, Dakota Madden-Fong, Brian Lantz

California Institute of Technology
LIGO Project, MS 18-34
Pasadena, CA 91125
Phone (626) 395-2129
Fax (626) 304-9834
E-mail: info@ligo.caltech.edu

Massachusetts Institute of Technology
LIGO Project, Room NW22-295
Cambridge, MA 02139
Phone (617) 253-4824
Fax (617) 253-7014
E-mail: info@ligo.mit.edu

LIGO Hanford Observatory
Route 10, Mile Marker 2
Richland, WA 99352
Phone (509) 372-8106
Fax (509) 372-8137
E-mail: info@ligo.caltech.edu

LIGO Livingston Observatory
19100 LIGO Lane
Livingston, LA 70754
Phone (225) 686-3100
Fax (225) 686-7189
E-mail: info@ligo.caltech.edu

http://www.ligo.caltech.edu/

Contents

1 Introduction

The purpose of this technical note is to expand upon Madeleine Waller's work with Norna Robertson during the summer of 2012 on the LIGO III quadruple pendulum conceptual design [1]. This document establishes some relatively simple but practical equations, based on some approximations and assumptions. These equations are used to optimize the longitudinal and vertical seismic isolation properties of the pendulum. This optimization is constrained by the payload limit of the BSC-ISI, the total length of the pendulum, and the desired test mass weight. The goal is to meet or beat the aLIGO quad performance. The

constraints and performance goals are detailed in Section 2.1.

These equations employed here are presented early, in the next section (Section 2.2), so they are readily available. The derivations of these equations are presented in detail in Appendices A and B. Discussions of optimizing these equations is presented in Section 2.3. Since no optimal solution exists that meets the performance goals within the constraints, Section 3 considers three modifications to the constraints and pendulum structure that do meet the performance goals. Table 3 summarizes the pendulum parameters for these solutions.

For most of this document we assume the LIGO III pendulum is similar to the aLIGO quad in construction. The only differences are the masses and the wires, and the use of silicon rather than silica. At the end of Section 3 we will break this assumption by considering springs at the penultimate mass.

This document follows the blue team design from the LIGO III strawman report [3], but the analysis is not restricted to this approach.

2 Parameter Optimization

This section presents a design process for the choosing parameters of the LIGO III quad conceptual design for longitudinal and seismic isolation performance. Some of these parameters also influence thermal noise performance. The parameters considered here, and sketched in Figure 1 include mass, wire length, and spring stiffness. Section 2.1 discusses the constraints on these parameters, and the assumptions behind those constraints. Section 2.2 introduces a minimal set of equations used to determine the optimal distribution of these parameters. Section 2.3 considers that some of these equations have competing optimal solutions, and outlines the problem of these competing goals.

2.1 Pendulum Design Constraints

The pendulum design is constrained to fit within certain weight and length limits. The relevant constraints for the equations in this section are the total main chain payload mass, total length, and test mass weight. Table 1 summarizes these constraints. To these constraints we add that the longitudinal seismic isolation, vertical seismic isolation, and the vertical bounce mode between the lowest two stages must perform as at least as well as the Advanced LIGO quad pendulum. These requirements are summarized in Table 2.

Table 1: LIGO III Quadruple pendulum parameter constraints. The total length in row 1 is defined from the suspension point to the center of the test mass. These values are based on the assumptions discussed in this section.

Parameter	Constraint	Value	Reference
$L_1 + L_2 + L_3 + L_4$	$\leq$	2.14 m	[1]
$P = m_1 + m_2 + m_3 + m_4$	$\leq$	270 kg	[2]
m_4	$=$	143 kg	[3]

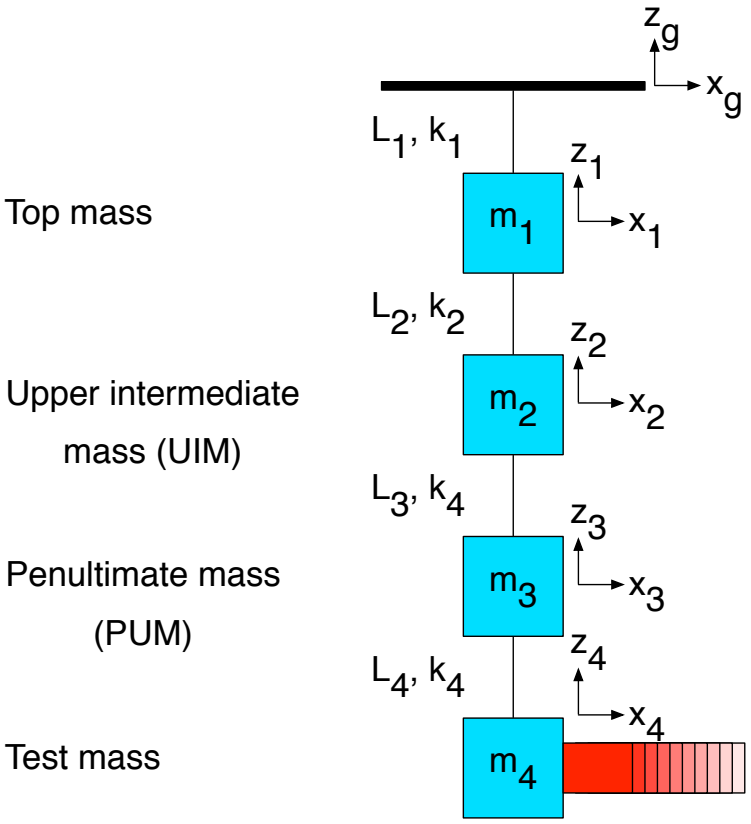

Figure 1: x_g and z_g represent longitudinal and vertical seismic motion respectively; x_1 to x_4 and z_1 to z_4 represent the motion of stages 1 to 4; m_1 to m_4 the mass of these stages; L_1 to L_4 the lengths of wire suspending these stages; and k_1 to k_4 the stiffnesses of these stages.

Table 2: Requirements based on current aLIGO quadruple pendulum performance. This document assumes that a LIGO III quad should meet or exceed the Advanced LIGO longitudinal and vertical seismic isolation.

Parameter	**Requirement**	**Value**	**Reference**
10 Hz longitudinal isolation	$\leq$	1.0875×10^{-7} m/m	[5]
10 Hz vertical isolation	$\leq$	1.3884×10^{-4} m/m	[5]
Vertical bounce mode	$\leq$	9.27 Hz	[5]

Table 1 states the total mass of the main chain must be no more than 270 kg [2]. This constraints assumes the BSC-ISI can handle 800 kg of total payload. Then (using educated guesses) it is assumed this 800 kg encompasses 300 kg in reserve for balancing, 60 kg for a reaction chain (scaled down from aLIGO by a factor 2), 20 kg for cryogenic equipment, 100 kg for a quadruple suspension cage (some of which may double as additional cryo equipment), and 50 kg for a Transmission Monitor suspension and cage. Some of these assumptions may be revisited in the future to fine tune the allowed main chain suspended mass.

The mass of the test mass is assumed fixed at 143 kg [3]. This high value was chosen by the Blue team in the LIGO III strawman report to minimize radiation pressure and thermal noise influences.

Table 2 adds to Table 1 by stating that a LIGO III quadruple pendulum performance should be at least as good as the Advanced LIGO pendulum. Here performance is defined in the first two rows as seismic isolation from BSC ISI stage 2 to the test mass in the longitudinal and vertical directions. The third row sets the performance of the highest frequency vertical mode. This mode represents bounce motion between the test mass and the penultimate mass, which tends to be at a high frequency due to the lack of springs between these stages. Keeping this mode low is good for both seismic isolation and thermal noise.

2.2 List of useful Equations

Eqs. (1) to (5) listed here are used to determine the optimal distribution of mass, wire length, and spring stiffness from the point of view of the quadruple pendulum longitudinal and vertical seismic isolation.

Longitudinal seismic isolation equations:

$$\frac{x_4}{x_g} \approx \frac{g^4}{(2\pi f)^8} \frac{1}{L_1 L_2 L_3 L_4} \frac{(m_1+m_2+m_3+m_4)(m_2+m_3+m_4)(m_3+m_4)m_4}{m_1 m_2 m_3 m_4} \tag{1}$$

$$m_2^* = -(m_3+m_4) + \sqrt{P(m_3+m_4)}, \quad P = m_1+m_2+m_3+m_4 \tag{2}$$

$$m_3^* = -A + A\sqrt{A+P-m_2-m_4}, \quad A = \frac{m_4(m_2+m_4)}{P+m_4} \tag{3}$$

Vertical seismic isolation equations:

$$\frac{z_4}{z_g} \approx \frac{1}{(2\pi f)^8} \frac{1}{m_1 m_2 m_3 m_4} k_1 k_2 k_3 k_4 \tag{4}$$

$$f_{bounce} \approx \frac{1}{2\pi} \sqrt{\frac{E_4 g}{L_4 \sigma_4} \left(1 + \frac{m_4}{m_3}\right)} \tag{5}$$

The subscript indices represent the stages in order of top to bottom, m represents mass in kg, L is wire length in m, g is gravity in m/s^2, f is frequency in Hz, k is stiffness in N/m, f_{bounce} is in units of Hz, σ_4 is the stress in the fibers between the PUM and test mass in Pa, and E_4 is the modulus of elasticity of those fibers in Pa.

Eq. (1), derived in Appendix A, is the high frequency asymptote of the longitudinal seismic transmission between BSC-ISI stage 2 displacement and test mass displacement. Used as an approximation, it is valid for all frequencies greater than the resonances, where the approximation error approaches zero as f approaches infinity. Figure 2 plots this approximation against the aLIGO model transfer function to provide an idea of where it is valid. Above the resonances, the approximation is an underestimate, as the seismic transmission approaches the asymptote from above.

Eqs. (2) and (3), derived in Appendix A, provide the optimal values of m_2 and m_3, m_2^* and m_3^* respectively. These values yield the minimum longitudinal seismic transmission from Equation (1) given the mass constraints in Table 1.

Eq. (4), derived in Appendix A, is the high frequency asymptote of the vertical seismic transmission between BSC-ISI stage 2 displacement and test mass displacement. Like, Equation (1), used as an approximation it is valid for all frequencies greater than the resonances, where the approximation error approaches zero as f approaches infinity. Figure 2 plots this approximation against the aLIGO model transfer function to provide an idea of where it is valid. Above the resonances, the approximation is an underestimate, as the seismic transmission approaches the asymptote from above.

Eq. (5), derived in Appendix B, is an approximation of the highest frequency vertical mode representing bounce motion between the bottom two stages. The error in Eq. (5) approaches zero when the distance between f_{bounce} and the second highest mode approaches infinity. As an idea of the accuracy of the equation, the aLIGO quad model has a bounce mode at 9.27 Hz with a second highest vertical mode at 3.56 Hz. The estimate of the bounce mode from Eq. (5) is 8.92 Hz. This is an error of 3.82%.

2.3 Optimization Discussion

Now that simple relations for seismic isolation have been obtained in Section 2.2 with their constraints in Section 2.1, we can proceed with searching them for the optimal values of mass, wire, length, and spring stiffness.

To begin the optimization, we first define what our goals are based on the requirements in Table 2. These are stated in the equations below,

from Eq. (1):

$$C_1 = \frac{g^4 P}{(2\pi f)^8} \min\left[\frac{1}{L_1 L_2 L_3 L_4} \frac{(m_2+m_3+m_4)(m_3+m_4)}{m_1 m_2 m_3}\right] \tag{6}$$

from Eq. (4):

$$C_2 = \frac{k_4}{m_4 (2\pi f)^8} \min\left[\frac{1}{m_1 m_2 m_3} k_1 k_2 k_3\right] \tag{7}$$

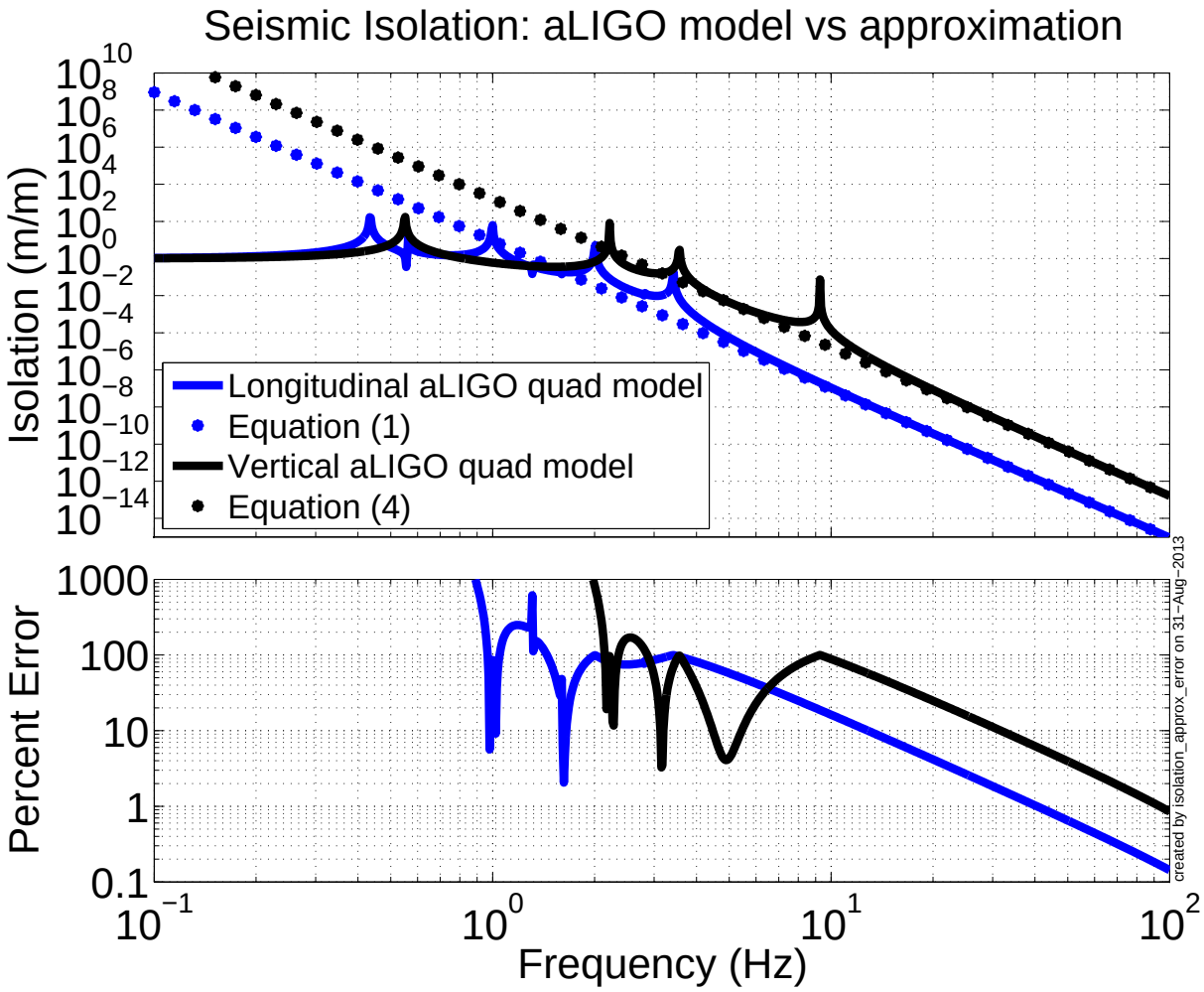

Figure 2: Comparison of Eq. (1) and Eq. (4) to the aLIGO quadruple pendulum model.

from Eq. (5):

$$C_3 = \frac{1}{2\pi}\sqrt{\frac{E_4 g}{\sigma_4}}\min\left[\sqrt{\frac{1}{L_4}\left(1+\frac{m_4}{m_3}\right)}\right] \tag{8}$$

where, C represents a cost term to be minimized. The index of each C corresponds to the respective row in Table 2.

The challenge is that each C must be considered simultaneously because the best solution for one is not necessarily the best solution for the others. We will first consider the solution for each C independently since this provides valuable insight into the behavior of the conceptual design. Then, we will try to search for parameters that simply meet all the design constraints and performance requirements simultaneously.

2.3.1 Solving C_1

Note that to find the solution of C_1 in Eq. 6 we can separate the wire length terms from the mass terms. Then, the optimal solution for the wire lengths is simply to make them all the same (to maximize $L_1L_2L_3L_4$), $2.14/4 = 0.535\,\mathrm{m}$.

The optimal solution of the mass values are determined from Eqs. (2) and (3) from Section 2.2. These equations provide the optimal solutions for m_2 or m_3 given all the other masses. To solve for both simultaneously, one must iterate between the two equations a few times.

Figures 3 and 4 plot an example of this iteration, with Figure 3 showing the convergence of the mass values, and Figure 4 showing the convergence of seismic isolation. One starts by guessing a value for m_3 (or m_2), solving for m_2^* (m_3^*), then solving a new m_3^* (m_2) with this m_2^* (m_3), and repeating. After just a few iterations, the values of m_2^* and m_3^* will converge to the values yielding best seismic isolation. Then, $m_1^* = P - m_4 - m_3^* - m_2^*$. The initial guess for this example is $m_3 = 80$ kg. This iteration is possible because Eq. (1) is convex in the parameter space of m_2 and m_3 (Appendix A.3.3). Given the constraint of a 143 kg test mass, this results in $m_3 = 33.74$ kg, $m_2 = 41.71$, $m_1 = 51.55$ kg, as shown in Figure 3. Appendix A confirms this result by using a numerical search to find the same values.

Note the trend of increasing mass going up the chain. This trend will always be the case for optimal longitudinal seismic isolation. The reason is because the longitudinal stiffness of a given wire is determined by weight hanging from it, as given by Eq. 31 in Appendix A.3.1. Thus, a lower stage's mass contributes to the stiffness of many stages while a higher stage contributes to few.

Plugging these values for the wire lengths and masses into Eq. 1, we get a seismic transmission at 10 Hz of 6.7×10^{-8} m/m (also shown in Figure 4). To check, plugging these into the model [5], we get 7.9×10^{-8} m/m. This performance is better than the aLIGO quad, which is 1.0875×10^{-7} m/m.

2.3.2 Solving C_2

The solution of C_2 is obtained by simple inspection. First, the mass values and stiffness values are separable. The goal is then to maximize the mass term while minimizing the

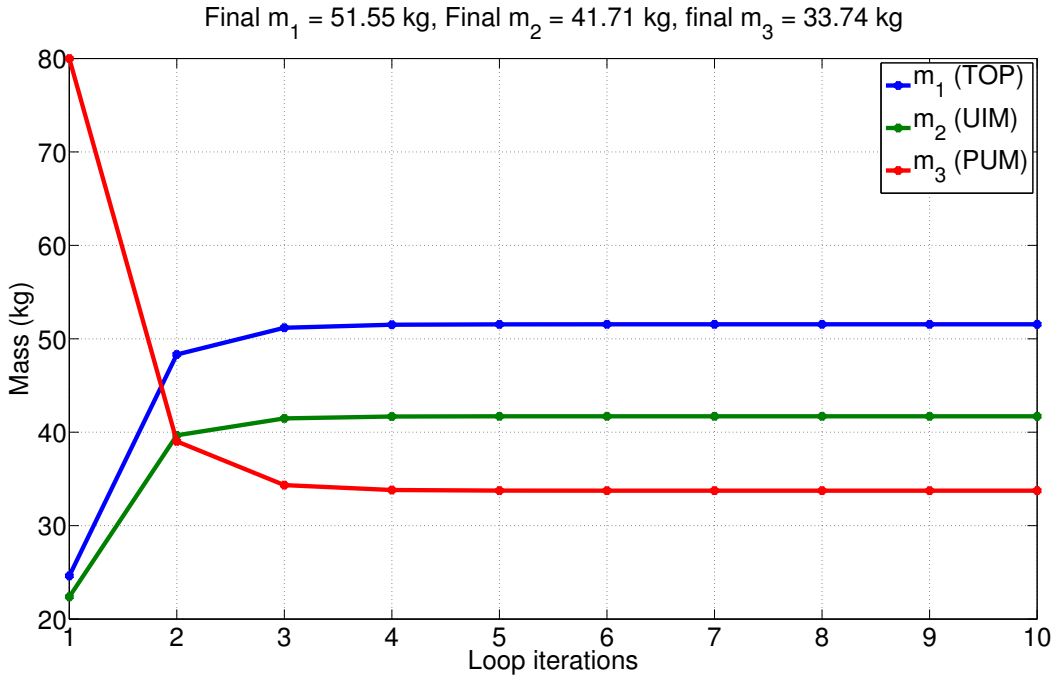

Figure 3: Solving the optimal mass values by iterating between Eqs. (2) and (2).

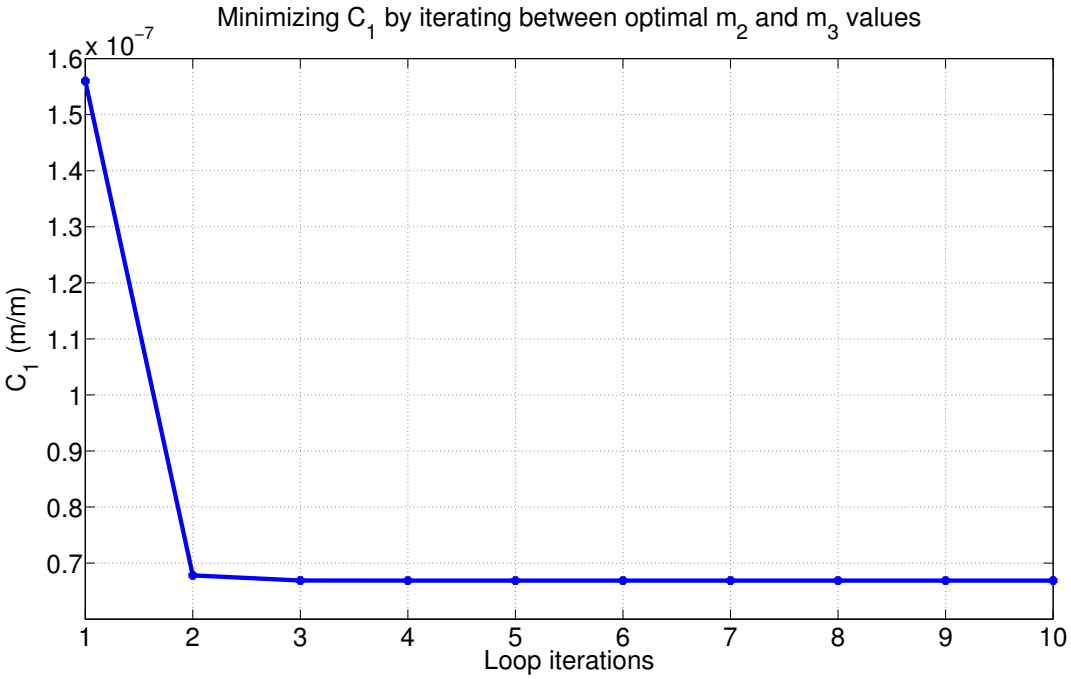

Figure 4: Solving the optimal mass values by iterating between Eqs. (2) and (2).

stiffness term. One optimizes the mass values by making them all the same, to maximize $m_1 m_2 m_3$. The stiffness values are optimized by making each one as small as possible through the geometry of the springs. In practice geometrical constraints limit the minimum stiffness.

Since these geometrical constraints are unknown to us, we will assume it is possible to design springs soft enough to meet the vertical seismic isolation requirement regardless of the mass and wire values. Thus, from this point on we will ignore C_2 and its corresponding vertical isolation requirement in the remainder of this document.

2.3.3 Solving C_3

The solution of C_3, the minimum bounce mode frequency, is also obtained by simple inspection. First, the wire length and mass terms are separable. The wire length terms are optimized by setting L_4, the test mass wires (or fibers) as long as possible. The mass term is optimized by making the penultimate mass value, m_3, as high as possible. Unlike C_1, there is no unique solution other than to make L_4 the entire suspension length, and m_3 the entire remaining suspension payload. Both extremes are clearly impractical. We'll consider the bounce mode together with the longitudinal isolation in the following section.

2.3.4 Considering C_1 and C_3 Simultaneously

Here we will first observe the resulting bounce mode from the parameters given by the solution of C_1 in Section 2.3.1. Then, we will turn it around, and solve for the m_3 that gives us a satisfactory bounce mode and observe the resulting best case longitudinal isolation. We will see how each case compares against the performance requirements. As stated in Section 2.3.2, we are ignoring C_2 and the corresponding vertical seismic isolation requirement by assuming that it is possible to design springs soft enough to meet this requirement regardless of the values selected for the mass and wire length parameters.

For the first case, we plug in the solution from C_1 in Section 2.3.1 into Eq. 5 and compare the result against the requirements in Table 2. Doing so, we get a bounce mode at 17.0 Hz (the exact model value would depend on the unknown spring stiffnesses). This value is well above the aLIGO value of 9.27 Hz, violating this requirement.

Note, the 17.0 Hz frequency was calculated by assuming a silicon modulus of elasticity at 120 K of 167.4 GPa [6], and a fiber stress of 1.4 GPa. There is still considerable uncertainty in what fiber stress is appropriate. Nonetheless, the fibers would have to be stressed nearly 4 times more to do better than the aLIGO quad given these masses and lengths.

For the second case, we'll try a longer wire length L_4 of 1 m, and observe what m_3 is required for the bounce mode to meet the aLIGO value. 1 m is chosen here since it is a value that has been considered before in [1]. Solving Eq. 5 for m_3 gives us Eq. 9. Then plugging in $L_4 = 1$ m, $m_4 = 143$ kg, and $f_{bounce} = 9.27$ Hz,

$$m_3 = m_4 \left[(2\pi f_{bounce})^2 \frac{L_4 \sigma_4}{E_4 g} - 1 \right]^{-1} \tag{9}$$

we get, $m_3 = 75.3$ kg. From this m_3, the optimal m_2 for longitudinal isolation is given by

Eq. 2 as 24.5 kg. 27.2 kg then remains for m_1.

The best 10 Hz longitudinal isolation we can get with these parameters, setting $L_1 = L_2 = L_3 = 1.14/3 = 0.38$ m, is 1.98×10^{-7} from Eq. 1 and 2.67×10^{-7} from the model, violating the longitudinal isolation goal by a factor of 2. Figure 5 tries this calculation for many different values of L_4. The curves demonstrate that it is not actually possible to meet both the longitudinal and bounce mode requirements simultaneously within these constraints. The best we can do is a model performance of 2.34×10^{-7} at $L_4 = 1.117$ m.

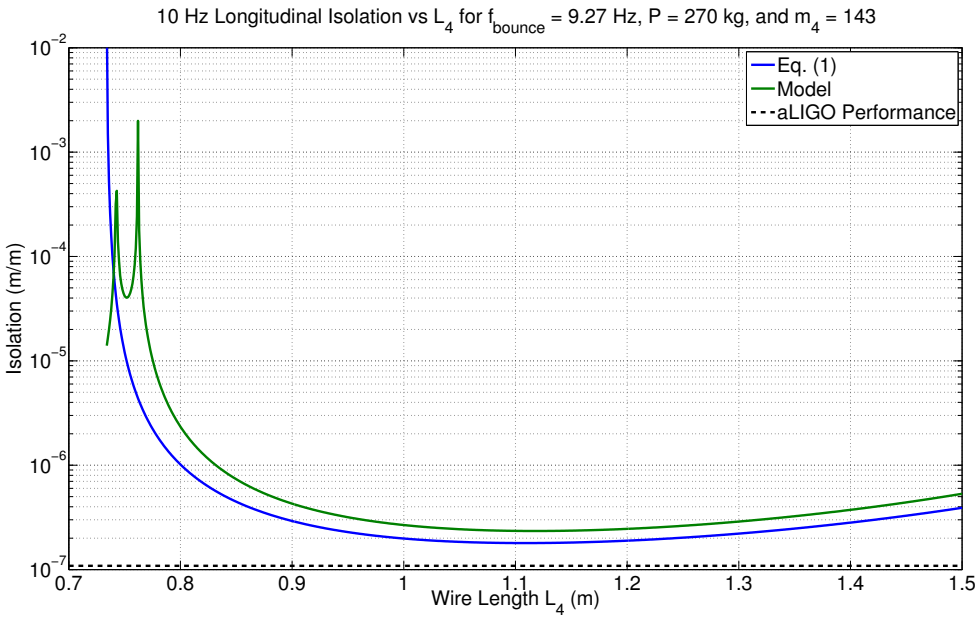

Figure 5: Optimal longitudinal isolation vs L_4. The bounce mode is fixed to meet the aLIGO performance. $L_1 = L_2 = L_3 = (2.14 - L_4)/3$.

3 Three Possible Solutions to Meet aLIGO Performance

As discussed in the previous section, it is not possible to design a LIGO III quadruple pendulum that performs as well as the aLIGO quad in terms of longitudinal isolation and bounce mode, given the constraints of a 270 kg payload, a 143 kg test mass, and a total wire length of 2.14 m. This section considers 3 possible modifications to these constraints, or to the structure of the pendulum itself, to make a pendulum that performs as well, if not better than, the aLIGO quad.

We assume the total wire length is truly fixed, as making a longer suspension would require unrealistic changes in the infrastructure at the observatories. However, we can consider increasing the total payload weight, decreasing the test mass weight, or adding springs to the penultimate mass. The parameters for these solutions are summarized in Table 3, and described in more detail in the following paragraphs.

First, let's consider allowing a greater payload P. This would permit more mass at the higher stages while keeping the same test mass weight, which would improve seismic isolation for

Table 3: Summary of model parameters for the three proposed modifications.

Parameters	**Increased** P	**Decreased** m_4	**Penultimate Springs**
P, Payload (kg)	301.9	270.0	270.0
m_1 (kg)	46.79	41.93	51.55
m_2 (kg)	39.54	35.42	41.71
m_3 (kg)	72.57	64.86	33.74
m_4 (kg)	143.0	127.8	143.0
L_1 (m)	0.372	0.372	0.535
L_2 (m)	0.372	0.372	0.535
L_3 (m)	0.372	0.372	0.535
L_4 (m)	1.025	1.025	0.535
long. isolation (m/m)	1.1×10^{-7}	1.1×10^{-7}	7.9×10^{-8}
f_{bounce} (Hz)	9.27	9.27	low, depends on springs
σ_4, fiber stress (Mpa)	1400	1400	1400
E_4, fiber modulus (Gpa) [6]	167.4	167.4	167.4
noise budget impact	none	slightly worse	better
relative cost	high	low	high

a given bounce mode. Figure 6 demonstrates the evolution of best longitudinal isolation against varying payload for $L_4 = 1\,\mathrm{m}$, $m_4 = 143$ kg, and $f_{bounce} = 9.27\,\mathrm{Hz}$. In this case, we need to increase the payload P by 32.3 kg to 302.3 kg in order to meet the aLIGO performance. The problem with a larger payload, is that the BSC-ISI would have to be reconfigured to hold the extra weight. Thus this solution, while possible, would require significant effort and cost, but it would not negatively impact the noise budget.

Second, the simplest solution is perhaps to employ a smaller test mass. Like the payload solution, a smaller test mass would improve seismic isolation for a given bounce mode. Figure 7 demonstrates the evolution of best longitudinal isolation against varying test mass weight for $L_4 = 1\,\mathrm{m}$, $P = 270$ kg, and $f_{bounce} = 9.27\,\mathrm{Hz}$. In this case, we need to decrease the test mass by 15.4 kg to 127.6 kg. Unlike the payload solution, this has the added benefits of a cheaper suspension without reworking the BSC-ISI. The cost we would pay would be in the noise budget. A smaller test mass would be more sensitive to radiation pressure and thermal noise. It might also be more difficult to maintain at cryogenic temperatures due to the reduced surface area.

In the first two solutions, we used a wire length of $L_4 = 1$ m to demonstrate how seismic isolation depends on the payload or test mass constraints while constraining the bounce mode. This wire length is not necessarily the best choice. Figure 8 shows the results of a search for the minimum possible payload, or the maximum possible test mass that meet the aLIGO quad performances for all wire lengths between 0.6 m and 1.5 m. The figure is generated by producing the curves of Figures 6 and 7 for many wire lengths. For each length, the mass values that provide the aLIGO seismic isolation are plotted in Figure 8. Thus, two things are learned from this plot. First, we see again that it is not possible to meet all the desired constraints and aLIGO performances simultaneously; and second, the closest we get is with $L_4 = 1.025$ m, resulting in a necessity to either increase the payload to 302 kg or decrease the test mass to 128 kg. Interestingly, this wire length is optimal for

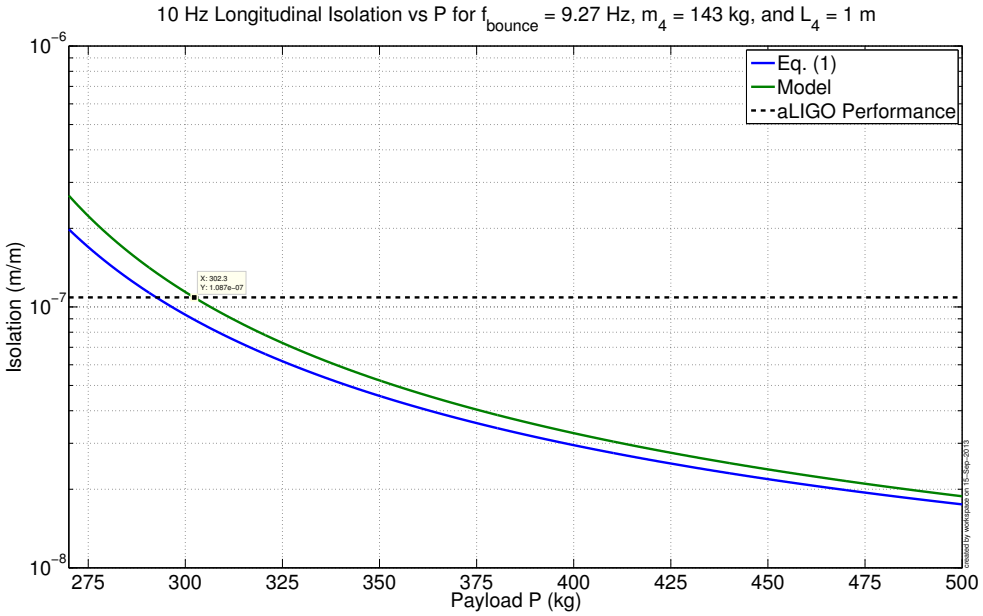

Figure 6: Optimal longitudinal isolation vs P. The bounce mode is fixed to meet the aLIGO performance by setting $m_3 = 75.34\,\mathrm{kg}$. $L_1 = L_2 = L_3 = 0.38\,\mathrm{m}$.

both the test mass weight and the total payload (not to mention being very close to the 1 m chosen in [1]). The suspension parameters that provide the optimal results for the two curves in Figure 8 are listed in Table 3.

For the third solution, instead of modifying weight constraints, let us now consider a modification to the pendulum structure. Up until now, we have assumed an aLIGO pendulum structure, but with modified masses, wire lengths, and silicon rather than silica. An additional change we can make, which is already being considered (by Glasgow?) is to add silicon springs at the penultimate mass. This change greatly simplifies the conceptual design because we are free to set the bounce mode with the springs. Thus, the bounce mode and longitudinal isolation problems decouple. We would chose whatever test mass size we like, set the other mass values according to Eqs. (2) and (3), choose the bounce mode with the silicon spring design, and be done. The optimal parameter values are listed in Table 3. In practice however, designing and implementing these springs is difficult and expensive, so all options need to be considered carefully.

An additional requirement for the suspensions is that all modes (except the two vertical and roll bounce modes) can be damped by the top mass damping loops. Figure 9 shows that for all three solutions all four longitudinal modes appear in the top mass to top mass transfer function. Thus, these modes can be damped by the top mass damping loops, satisfying the requirement for the longitudinal degree of freedom. The coupling of the vertical modes will depend on the spring stiffnesses chosen. It should be pointed out that an additional advantage of adding blade springs to the penultimate mass is that the two otherwise undampable bounce modes can be made to couple to the top mass, permitting their damping as well.

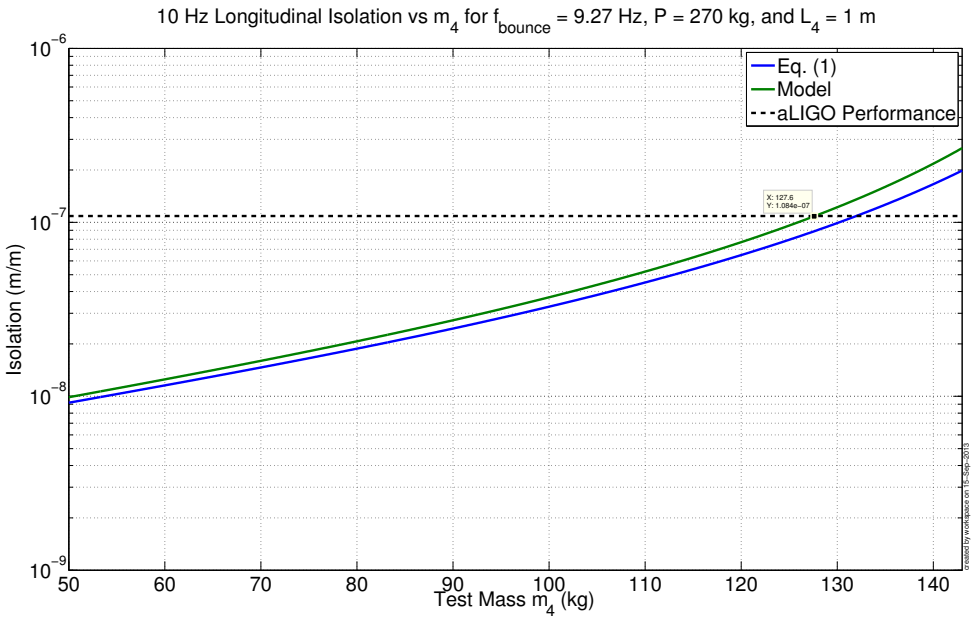

Figure 7: Optimal longitudinal isolation vs P. The bounce mode is fixed to meet the aLIGO performance. $L_1 = L_2 = L_3 = 0.38\,\mathrm{m}$.

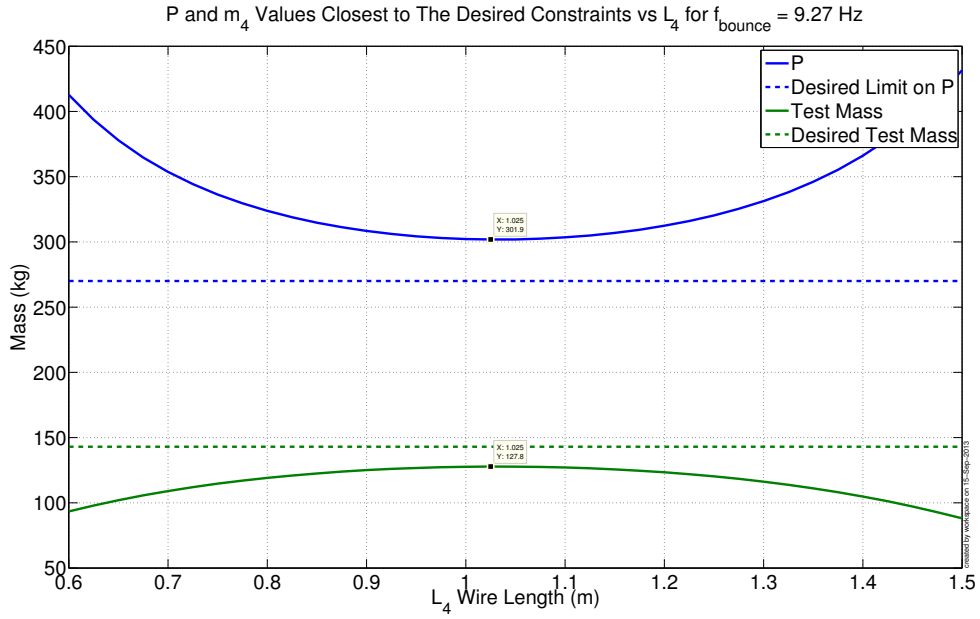

Figure 8: Releasing constraints: The blue curve is the value of P that meets the aLIGO longitudinal isolation for $m_4 = 143\,\mathrm{kg}$. The green curve is the value of m_4 that meets the aLIGO longitudinal isolation for $P = 270$.

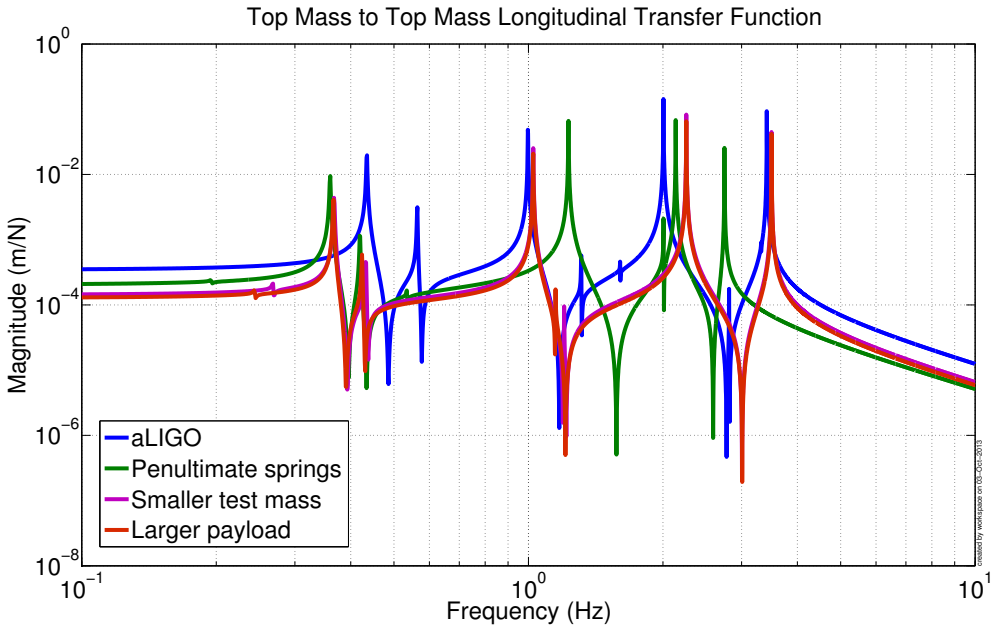

Figure 9: Top mass to top mass longitudinal transfer functions showing that all 4 longitduinal modes are visible at the top mass in all three solutions. Since all longitudinal modes are visible, the damping loops have access to them. Note, the purple curve is partially obstructed by the red curve.

4 Conclusion

This technical note develops mathematical tools for optimizing the performance of a LIGO III quadruple pendulum in terms of longitudinal and vertical seismic isolation and bounce mode frequency. From these tools, the optimal longitudinal isolation is given by unique set of wire lengths and mass values. The vertical isolation can be set arbitrarily by design of the spring stiffness values. The bounce mode is moved down in frequency either by increasing the lowest wire length or by minimizing the ratio of test mass to penultimate mass weight.

Assuming an aLIGO structure to the pendulum, it is not possible to reconcile the longitudinal isolation and bounce mode frequency such that they perform at least as well as the aLIGO quad given our current constraints of payload, wire length, and test mass weight. To improve the performance, the document suggests 3 possible solution: 1) allow for greater payloads, 2) reduce the test mass weight, or 3) install springs at the test mass. All of these solutions have pros or cons. 1) and 3) have better noise performance (the latter is best), but come at significant cost. 2) has slightly worse noise performance, but is the cheapest. All the trade-offs need careful consideration when deciding which approach is best.

Note, an important parameter that contains significant uncertainty, and that influences these results is the maximum stress we can apply to the silicon fibers. The higher the allowable stress, the easier the other requirements are to meet. Consequently, it is critical we put tight bounds on this stress moving forward.

A Seismic Isolation Derivations

This appendix derives the longitudinal and vertical seismic isolation Eqs. (1) to (4) in Section 2.2. Section A.1 introduces a generalized single axis 4 stage system, which will be analyzed in Section A.2 to derive the asymptotes of the longitudinal and vertical seismic isolation transfer functions. Section A.3 finds the set of masses that optimizes the longitudinal isolation derived in Section A.2.

The notation in this appendix and the next follows these conventions:

- Bold upper case letters, e.g. $\mathbf{M}$, denote matrices.
- Bold lower case letters, e.g. $\mathbf{x}$, denote vectors. All vectors are column vectors.
- Non-bold lower or upper case letters, e.g. ω, denote scalar values.
- Subscripts on scalars, e.g. m_1, refer to the pendulum stage, 1 through 4 top down
- Subscripts on matrices, e.g. $\mathbf{C}_{14}$, refer to the row and column of a matrix element.

A.1 Generalized System

This section presents the general 4 stage single-axis mass spring system shown in Figure 10. This system's equations of motion, described here, are important for the seismic isolation derivations in A.2.

Simplifying a four stage quadruple pendulum to movement along a single axis (longitudinal, vertical, etc) is a powerful tool in understanding its behavior and performance. The equations of motion become much more tractable, yet have sufficient detail to accurately reproduce seismic isolation properties (some of the highly coupled DOFs like transverse and roll cannot accurately be simplified to single axis systems).

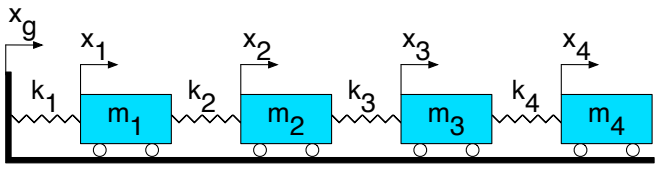

Figure 10: This single-axis mass spring system is used to simplify and generalize the dynamics of the quadruple pendulum. x_g represents ground motion, x_1 to x_4 represents the motion of stages 1 to 4, m_1 to m_4 the mass of these stages, and k_1 to k_4 the stiffnesses of these stages.

The system in Figure 10 consists of 4 masses, m_1 to m_4 constrained to move along a single axis, the x axis. In this general system, x could be thought of as any DOF, e.g. longitudinal, vertical, etc. The ground is also constrained to move along this axis. The masses are connected to the ground and to each other by springs k_1 to k_4.

The dynamics of this system are governed by the following equations of motion

$$\mathbf{M}\ddot{\mathbf{x}} + \mathbf{K}\mathbf{x} = \begin{bmatrix} k_1 \\ \mathbf{0}_{3\times 1} \end{bmatrix} x_g \tag{10}$$

$$\mathbf{M} = \begin{bmatrix} m_1 & 0 & 0 & 0 \\ 0 & m_2 & 0 & 0 \\ 0 & 0 & m_3 & 0 \\ 0 & 0 & 0 & m_4 \end{bmatrix} \tag{11}$$

$$\mathbf{K} = \begin{bmatrix} k_1 + k_2 & -k_2 & 0 & 0 \\ -k_2 & k_2 + k_3 & -k_3 & 0 \\ 0 & -k_3 & k_3 + k_4 & -k_4 \\ 0 & 0 & -k_4 & k_4 \end{bmatrix} \tag{12}$$

$$\mathbf{x} = \begin{bmatrix} x_1 \\ x_2 \\ x_3 \\ x_4 \end{bmatrix} \tag{13}$$

where, $\mathbf{M}$ is the diagonal mass matrix, $\mathbf{K}$ is the symmetric positive definite stiffness matrix, and $\mathbf{x}$ is the vector of displacement coordinates for the four masses.

Note, the derivation of $\mathbf{K}$ can be obtained by inspection of Figure 10 using Hooke's Law, $\mathbf{f} = \mathbf{K}\mathbf{x}$. The procedure is the following: move x_1 by a unit displacement while holding the other masses fixed. The forces on each mass required to hold this configuration yield the first column of $\mathbf{K}$; then repeat this procedure moving each stage by unit displacements one at a time until the full matrix is constructed.

A.2 Derivation of General Single-Axis Seismic Isolation

For the system described in A.1, this section will derive the transmission of x_g to x_4 as

$$\frac{x_4}{x_g} \approx \frac{1}{(2\pi f)^8} \frac{k_1 k_2 k_3 k_4}{m_1 m_2 m_3 m_4} \tag{14}$$

where f is the frequency in Hz, for frequencies greater than the resonance frequencies.

First, we take the generalized equation of motion in Eq. 10 and multiply both sides by the inverse of $\mathbf{M}$.

$$\ddot{\mathbf{x}} + \mathbf{M}^{-1}\mathbf{K}\mathbf{x} = \begin{bmatrix} k_1/m_1 \\ \mathbf{0}_{3\times 1} \end{bmatrix} x_g \tag{15}$$

Then we take the Laplace Transform of both sides where s is the Laplacian variable.

$$\mathbf{x}s^2 + \mathbf{M}^{-1}\mathbf{K}\mathbf{x} = \begin{bmatrix} k_1/m_1 \\ \mathbf{0}_{3\times 1} \end{bmatrix} x_g \tag{16}$$

Solving for $\mathbf{x}$,

$$\mathbf{x} = \left[\mathbf{M}^{-1}\mathbf{K} + s^2\mathbf{I}_{4\times4}\right]^{-1} \begin{bmatrix} k_1/m_1 \\ \mathbf{0}_{3\times1} \end{bmatrix} x_g \tag{17}$$

To find the magnitude and phase relation between x_g and x_4 we set s to,

$$s = i\omega \tag{18}$$

where i is the imaginary number, and w is the frequency in radians/second. As an aside, setting $s = i\omega$ converts the Laplace Transform to the Fourier Transform.

$$\mathbf{x} = \left[\mathbf{M}^{-1}\mathbf{K} - \omega^2\mathbf{I}_{4\times4}\right]^{-1} \begin{bmatrix} k_1/m_1 \\ \mathbf{0}_{3\times1} \end{bmatrix} x_g \tag{19}$$

Set an intermediate variable $\mathbf{V}$ as the matrix that gets inverted,

$$\mathbf{V} = \left[\mathbf{M}^{-1}\mathbf{K} - \omega^2\mathbf{I}_{4\times4}\right] \tag{20}$$

$$\mathbf{V} = \begin{bmatrix} \frac{k_1+k_2}{m_1} - \omega^2 & \frac{-k_2}{m_1} & 0 & 0 \\ \frac{-k_2}{m_2} & \frac{k_2+k_3}{m_2} - \omega^2 & \frac{-k_3}{m_2} & 0 \\ 0 & \frac{-k_3}{m_3} & \frac{k_3+k_4}{m_3} - \omega^2 & \frac{-k_4}{m_3} \\ 0 & 0 & \frac{-k_4}{m_4} & \frac{k_4}{m_4} - \omega^2 \end{bmatrix} \tag{21}$$

$$\mathbf{x} = \mathbf{V}^{-1} \begin{bmatrix} k_1/m_1 \\ \mathbf{0}_{3\times1} \end{bmatrix} x_g \tag{22}$$

This matrix is difficult to invert analytically, but for the ground to test mass isolation, all we need is the lower left element (index 4,1) of $\mathbf{V}^{-1}$. Thus we don't need to invert the whole matrix. This element is equal to

$$(\mathbf{V}^{-1})_{41} = \frac{1}{|\mathbf{V}|}\mathbf{C}_{14} \tag{23}$$

Where $\mathbf{C}$ is the matrix of cofactors. The $\mathbf{C}_{14}$ element is equal to the negative determinant of the 3×3 lower left corner of $\mathbf{V}$ [4].

$$\mathbf{C}_{14} = -\begin{vmatrix} \frac{-k_2}{m_2} & \frac{k_2+k_3}{m_2} - \omega^2 & \frac{-k_3}{m_2} \\ 0 & \frac{-k_3}{m_3} & \frac{k_3+k_4}{m_3} - \omega^2 \\ 0 & 0 & \frac{-k_4}{m_4} \end{vmatrix} = \frac{k_2 k_3 k_4}{m_2 m_3 m_4} \tag{24}$$

Note, $\mathbf{C}_{14}$ is a triangular matrix, so its determinant is simply the product of the diagonal.

Up to this point we have made no approximations. To find the determinant of $\mathbf{V}$ for Eq. 23 we assume high frequencies, where $\omega >$ resonance frequencies. In this regime, $\mathbf{V}$ approaches the diagonal matrix

$$\mathbf{V} \approx \begin{bmatrix} -\omega^2 & 0 & 0 & 0 \\ 0 & -\omega^2 & 0 & 0 \\ 0 & 0 & -\omega^2 & 0 \\ 0 & 0 & 0 & 0 - \omega^2 \end{bmatrix} \tag{25}$$

Thus, the determinant of $\mathbf{V}$ at these high frequencies is

$$|\mathbf{V}| \approx \omega^8 \tag{26}$$

Putting this together with Eq. 22 gives us,

$$\boxed{\frac{x_4}{x_g} = \frac{1}{\omega^8} \frac{k_1 k_2 k_3 k_4}{m_1 m_2 m_3 m_4}} \tag{27}$$

Finally, plugging in $\omega = 2\pi f$ yields Eq. 14, the transmission of seismic noise through the system. This equation can be used directly for the quadruple pendulum vertical isolation, where the k values become the net blade spring stiffness at each stage.

A.3 Derivation of Optimal Longitudinal Isolation

This section derives the set of mass values for a quadruple pendulum that provide the best longitudinal isolation for a given payload. For this calculation we use Eq. 14.

A.3.1 Longitudinal Stiffness Derivation

To use Eq. 14 for longitudinal isolation we must first derive the k values. Figure 11 illustrates an arbitrary mass of mass m suspended from a wire of length L, and supporting a vertical load f_{load}. The mass is displaced in the longitudinal direction a distance x. This displacement causes the wire to pivot an angle θ. To find the stiffness, we need the restoring force, $f_{restore}$, as a function of displacement x. This restoring force is

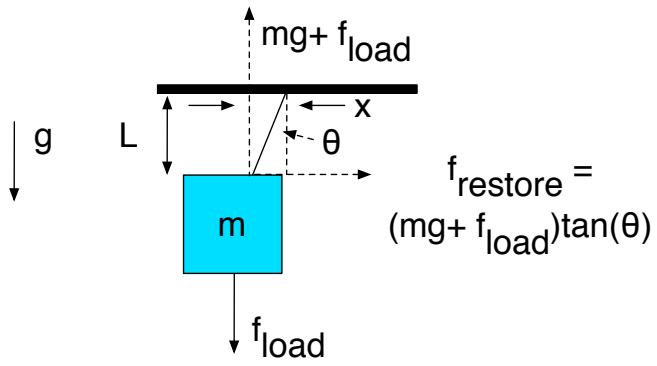

Figure 11: Sketch of the forces on a suspended stage of mass m hanging from a wire of length L at an angle θ.

$$f_{restore} = (mg + f_{load}) \tan\theta \tag{28}$$

But, for small angles,

$$f_{restore} \approx (mg + f_{load}) \frac{x}{L} \tag{29}$$

Therefore,

$$k \approx \frac{f_{restore}}{x} = \frac{(mg + f_{load})}{L} \tag{30}$$

Thus, the stiffness for a suspended mass can be stated simply as the tension in the wire divided by the wire length. In general, for an N stage pendulum,

$$k_i = g \frac{\sum_i^N m_i}{L_i} \tag{31}$$

where i is the index of the stage in order of top down. Plugging this into Eq. 14 we get,

$$\boxed{\frac{x_4}{x_g} = \frac{g^4}{(2\pi f)^8} \frac{1}{L_1 L_2 L_3 L_4} \frac{(m_1 + m_2 + m_3 + m_4)(m_2 + m_3 + m_4)(m_3 + m_4)m4}{m_1 m_2 m_3 m_4}} \tag{32}$$

We can minimize this function to optimize the isolation. Note that the minimization over the wire lengths is separable from that of the masses. The optimal wire lengths are obtained when they are all equal segments of the total suspension length. The optimal solution for the masses is somewhat more complicated and derived in detail in Section A.3.2.

A.3.2 Optimal Masses

The goal is to minimize Eq. 32 with respect to the four mass parameters. First, note that by invoking our two mass constraints we can reduce this four parameter minimization to two parameters.

$$m_4 = 143 \tag{33}$$

$$m_1 = P - m_2 - m_3 - m_4 \tag{34}$$

where $P = m_1 + m_2 + m_3 + m_4 = 270\,\mathrm{kg}$. Then,

$$\frac{x_4}{x_g} = \frac{g^4}{(2\pi f)^8}\frac{P}{L_1L_2L_3L_4}\left[\frac{(m_2+m_3+m_4)(m_3+m_4)}{(P-m_2-m_3-m_4)m_2m_3}\right] \tag{35}$$

where the term in the square brackets is to be minimized with respect to m_2 and m_3. Thus, we can restate the minimization problem as

$$\min\left[\frac{N}{D}\right] \tag{36}$$

where N is the numerator and D is the denominator,

$$N = m_2m_3 + m_2m_4 + 2m_3m_4 + m_3^2 + m_4^2 \tag{37}$$

$$D = Pm_2m_3 - m_2^2m_3 - m_2m_3^2 - m_2m_3m_4 \tag{38}$$

Then, minimizing by setting the derivative with respect to m_i to 0,

$$\frac{\partial}{\partial m_i}\left[\frac{N}{D}\right] = \left(\frac{\partial}{\partial m_i}N\right)D^{-1} + N\left(\frac{\partial}{\partial m_i}D^{-1}\right) = 0 \tag{39}$$

$$\left(\frac{\partial}{\partial m_i}N\right)D^{-1} - ND^{-2}\left(\frac{\partial}{\partial m_i}D\right) = 0 \tag{40}$$

multiply both sides by D

$$\left(\frac{\partial}{\partial m_i}N\right) - ND^{-1}\left(\frac{\partial}{\partial m_i}D\right) = 0 \tag{41}$$

put derivatives on the left and everything else on the right,

$$\frac{\partial N/\partial m_i}{\partial D/\partial m_i} = \frac{N}{D} \tag{42}$$

Then to solve for the optimal m_2 and m_3 values, we solve $\partial N/\partial m_i$ and $\partial D/\partial m_i$ for $i = 2$ and $i = 3$ respectively.

$$\frac{\partial N}{\partial m_2} = m_3 + m_4, \quad \frac{\partial D}{\partial m_2} = Pm_3 - 2m_2m_3 - m_3^2 - m_3m_4 \tag{43}$$

$$\frac{\partial N}{\partial m_3} = m_2 + 2m_3 + 2m_4, \quad \frac{\partial D}{\partial m_3} = Pm_2 - m_2^2 - 2m_2m_3 - m_2m_4 \tag{44}$$

We choose to solve for the optimal m_2 first. For m_2, Eq. 42 is

$$\frac{m_3+m_4}{Pm_3-2m_2m_3-m_3^2-m_3m_4}=\frac{(m_2+m_3+m_4)(m_3+m_4)}{(P-m_2-m_3-m_4)m_2m_3} \tag{45}$$

Both sides contain $\frac{m_3+m_4}{m_3}$, so we cancel those terms out,

$$\frac{1}{P-2m_2-m_3-m_4}=\frac{m_2+m_3+m_4}{(P-m_2-m_3-m_4)m_2} \tag{46}$$

Then, cross multiply the fractions to get the equation on a single line,

$$(P-m_2-m_3-m_4)m_2=(P-2m_2-m_3-m_4)(m_2+m_3+m_4) \tag{47}$$

Restate the equation in a quadratic form with respect to m_2

$$m_2^2+2(m_3+m_4)m_2-(m_3+m_4)(P-m_3-m_4)=0 \tag{48}$$

Then the solutions for m_2 are

$$m_2=-(m_3+m_4)\pm 0.5\sqrt{4(m_3+m_4)^2+4(m_3+m_4)(P-m_3-m_4)} \tag{49}$$

Simplifying, and noting that the negative square root solution is invalid because it yields negative mass, the final result for the optimal m_2, m_2^*, is

$$\boxed{m_2^*=-(m_3+m_4)+\sqrt{P(m_3+m_4)}} \tag{50}$$

Now to solve for the optimal m_3, Eq. 42 is

$$\frac{m_2+2m_3+2m_4}{Pm_2-m_2^2-2m_2m_3-m_2m_4}=\frac{(m_2+m_3+m_4)(m_3+m_4)}{(P-m_2-m_3-m_4)m_2m_3} \tag{51}$$

Both sides contain $\frac{1}{m_2}$, so canceling that out,

$$\frac{m_2+2m_3+2m_4}{P-m_2-2m_3-m_4}=\frac{(m_2+m_3+m_4)(m_3+m_4)}{(P-m_2-m_3-m_4)m_3} \tag{52}$$

Then, cross multiply the fractions to get the equation on a single line,

$$(m_2+2m_3+2m_4)(P-m_2-m_3-m_4)m_3=(P-m_2-2m_3-m_4)(m_2+m_3+m_4)(m_3+m_4) \tag{53}$$

Restate the equation in a quadratic form with respect to m_3 (the m_3^3 terms cancel out)

$$m_3^2+\frac{2m_4(m_2+m_4)}{P+m_4}m_3-\frac{m_4(m_2+m_4)(P-m_2-m_3)}{P+m_4}=0 \tag{54}$$

Then, the only valid solution for the optimal m_3, m_3^*, is,

$$\boxed{m_3^* = -A + \sqrt{A^2 + A(P - m_2 - m_4)}} \tag{55}$$

where,

$$A = \frac{m_4(m_2 + m_4)}{P + m_4} \tag{56}$$

As described in Section 2.3.1, m_2^* and m_3^* can be solved simultaneously by iterating the two equations. For $P = 270$ kg and $m_4 = 143$ kg, this results in $m_2^* = 41.71$ kg, $m_3^* = 33.74$ kg, leaving 51.55 kg for m_1. To check that this solution is correct, we can do a brute force scan of the m_2 and m_3 parameter space in the MATLAB model and observe if the same values are obtained for the best longitudinal seismic isolation. Figure 12 performs such a scan using the full quad model. First, we can see that the isolation is convex (bowl shaped, see Section A.3.3) in this parameter space, which is a sufficient condition to permit the previous solution by iteration. Second, the optimal values obtained are $m_1 = 51.67$ kg, $m_2 = 42.65$ kg, $m_3 = 33.68$ kg. These equal the calculated values within the 0.2345 kg plot resolution.

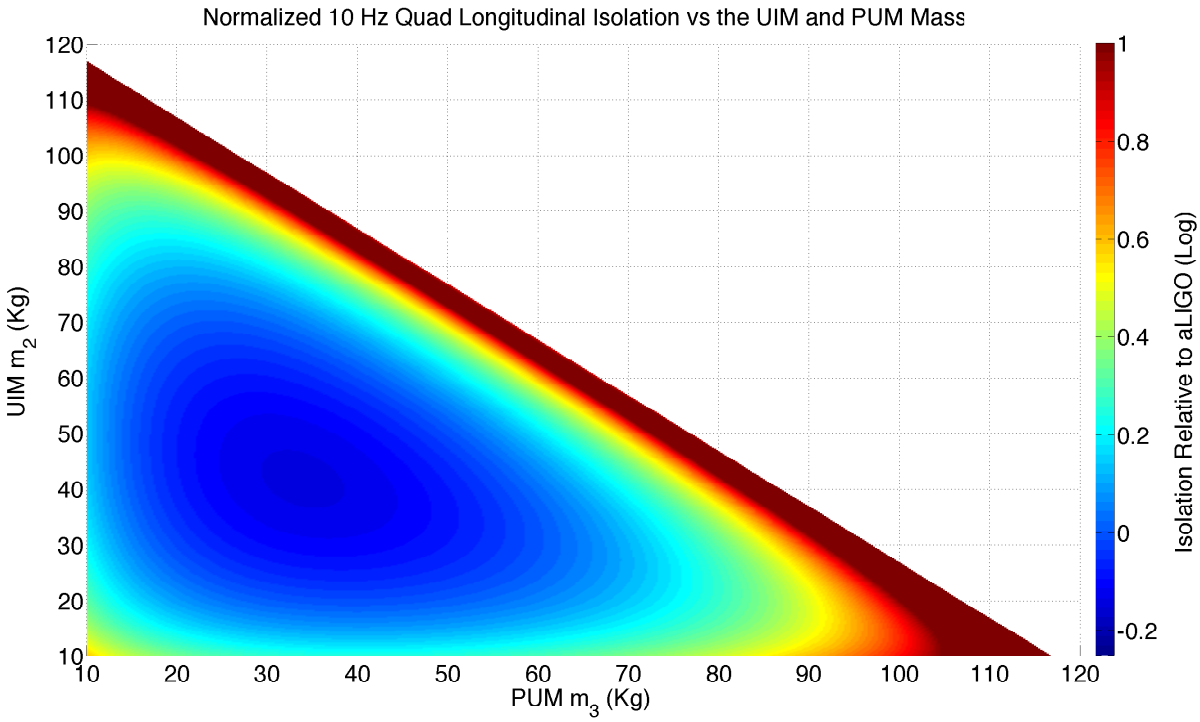

Figure 12: Scanning the LIGO III quad model with the m_2 and m_3 values. The color axis is the log of the 10 Hz longitudinal seismic transmission normalized by the aLIGO transmission, e.g. 0 is equal to aLIGO, 1 is 10 times worse. $m_1 = 270 - m_2 - m_3 - m_4$, where $m_4 = 143$. The wire lengths are all 0.535 m. The minimum transmission occurs at $m_1 = 51.67$, $m_2 = 42.65$, $m_3 = 33.68$. The plot has a mass resolution of 0.2345 kg.

A.3.3 Convexity Check for m_2 and m_3 Parameter Space

In Sections 2.3.1 and A.3.2, it was mentioned that the optimal m_2 and m_3 values for longitudinal isolation can be solved simultaneously by iterating between Eqs. (2) and (3). The validity of this iteration is proved by showing that the problem of minimizing m_2 and m_3 is convex, i.e. the longitudinal isolation curve is a bowl shaped function of these parameters. In other words, there is only 1 local minimum and nowhere does the slope with respect to these parameters go to zero except at this minimum.

The minimization problem is shown to be convex by showing that the Hessian matrix (matrix of second derivatives) of the longitudinal isolation is positive definite over the entire feasible parameter space. This is analogous to the one dimensional problem of proving that the extremum (flat part) of a function is a unique minimum by showing that its second derivative is positive everywhere (parabola for example). A number of ways exist to show that a matrix is positive definite. In this case we will use the property that all eigenvalues are positive [4].

To start the derivation of second derivatives we can pick up from the derivation of the gradients in Eq. (40). Denoting the Hessian matrix as $\mathbf{H}$,

$$H_{ij} = \frac{\partial}{\partial m_j}\left[\left(\frac{\partial}{\partial m_i}N\right)D^{-1} - ND^{-2}\left(\frac{\partial}{\partial m_i}D\right)\right] \tag{57}$$

where H_{ij} refers to the $i_{th}-1$ row and $j_{th}-1$ column of $\mathbf{H}$, and i and j are indices representing the pendulum stage numbers from 2 to 3. Carrying through the partial derivate of m_j,

$$H_{ij} = \frac{\partial^2 N}{\partial m_i \partial m_j}D^{-1} - \frac{\partial N}{\partial m_i}\frac{\partial D}{\partial m_j}D^{-2} - \frac{\partial^2 D}{\partial m_i \partial m_j}ND^{-2} - \frac{\partial D}{\partial m_i}\frac{\partial N}{\partial m_j}D^{-2} + 2\frac{\partial D}{\partial m_i}\frac{\partial N}{\partial m_j}ND^{-3} \tag{58}$$

Since pulling out constant positive terms will not effect the positive definiteness of $\mathbf{H}$, we can make the simplification that $\bar{\mathbf{H}} = \mathbf{H}D^3$ and study the positive definiteness of $\bar{\mathbf{H}}$ instead.

$$\bar{H}_{ij} = \frac{\partial^2 N}{\partial m_i \partial m_j}D^2 - \frac{\partial N}{\partial m_i}\frac{\partial D}{\partial m_j}D - \frac{\partial^2 D}{\partial m_i \partial m_j}ND - \frac{\partial D}{\partial m_i}\frac{\partial N}{\partial m_j}D + 2\frac{\partial D}{\partial m_i}\frac{\partial N}{\partial m_j}N \tag{59}$$

Solving for the second derivatives of N and D, picking up from the first derivatives in Eqs. (43) and (44),

$$\frac{\partial^2 N}{\partial m_2^2} = 0, \quad \frac{\partial^2 D}{\partial m_2^2} = -2m_3 \tag{60}$$

$$\frac{\partial^2 N}{\partial m_2 \partial m_3} = 1, \quad \frac{\partial^2 D}{\partial m_2 \partial m_3} = P - 2m_2 - 2m_3 - m_4 \tag{61}$$

$$\frac{\partial^2 N}{\partial m_3 \partial m_2} = 1, \quad \frac{\partial^2 D}{\partial m_3 \partial m_2} = P - 2m_2 - 2m_3 - m_4 \tag{62}$$

$$\frac{\partial^2 N}{\partial m_3^2} = 2, \quad \frac{\partial^2 D}{\partial m_3^2} = -2m_2 \tag{63}$$

We then need to show that all eigenvalues of $\bar{\mathbf{H}}$ are positive in the entire parameter space. While there may very well be an analytical proof, finding one proved challenging. Thus, using MATLAB, we calculate $\bar{\mathbf{H}}$ for many values of m_2 and m_3 and plot the smallest eigenvalue at each point. Figure 13 plots these results for the constraints of $P = 270$ kg and $m_4 = 143$ kg. m_1, m_2, m_3 are also constrained to be no less than 10 kg. Within these constraints, the smallest eigenvalue is always positive. Interestingly, if m_1, m_2, or m_3 shrink all the way to 0, than a 0 eigenvalue is found, however reality requires masses with greater than zero size.

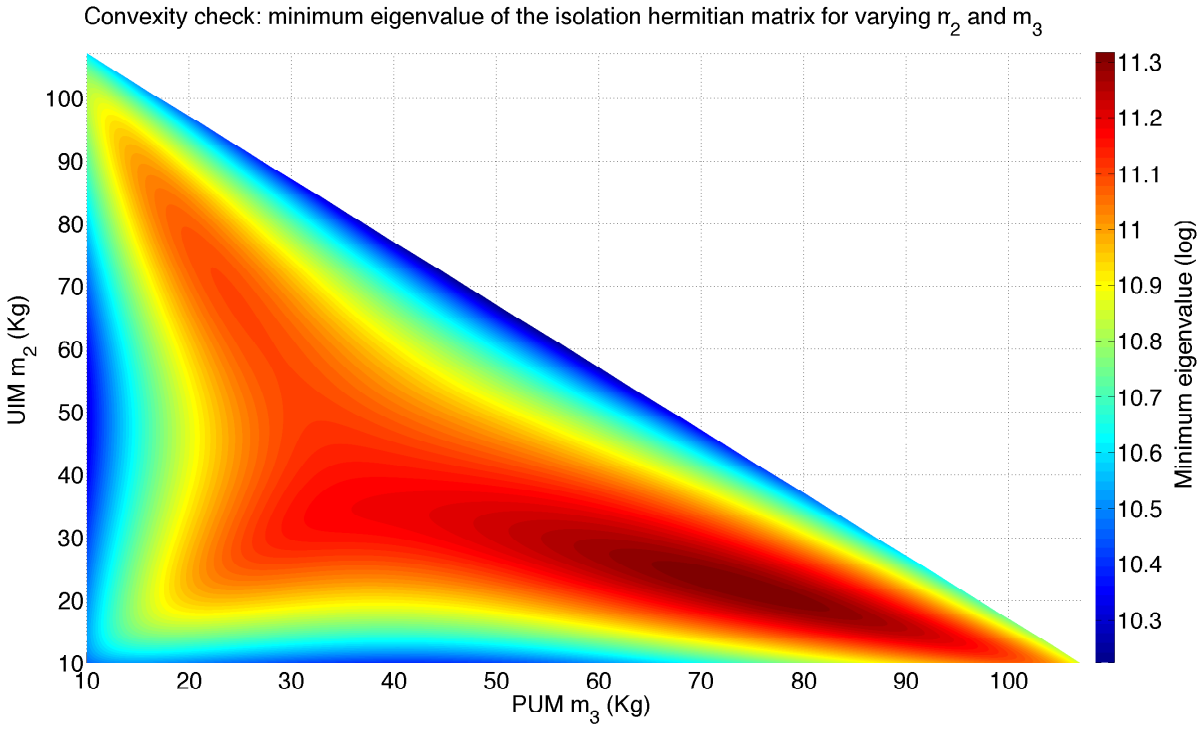

Figure 13: Scanning the LIGO III quad model with the m_2 and m_3 values. The color axis is the log of the smallest eigenvalue (in the pair) of $\bar{\mathbf{H}}$ at each point in the parameter space. The parameter space is constrained so the no mass is ever less than 10 kg when the payload $P = 270$ kg and the test mass $m_4 = 143$ kg. All eigenvalues within these constraints are greater than zero, indicating that the minimization of longitudinal isolation over m_2 and m_3 is convex. The minimum eigenvalue would go to zero as a stage approaches 0 kg, but we have imposed the more reasonable constraint of a 10 kg minimum.

We also consider the possibility of changing the payload and test mass constraints and show that all eigenvalues still remain positive for any reasonable constraint combination. Figure 14 plots these results. The figure is constructed essentially by compiling many plots like Figure 13 for a variety of payload and test mass constraints. In each case the minimum eigenvalue in each plot is recorded. Figure 14 shows the minimum value from each of these plots. In all cases, the eigenvalues remain positive. Thus, the simultaneous solution of m_2 and m_3 by iterating Eqs. (2) and (3) is optimal.

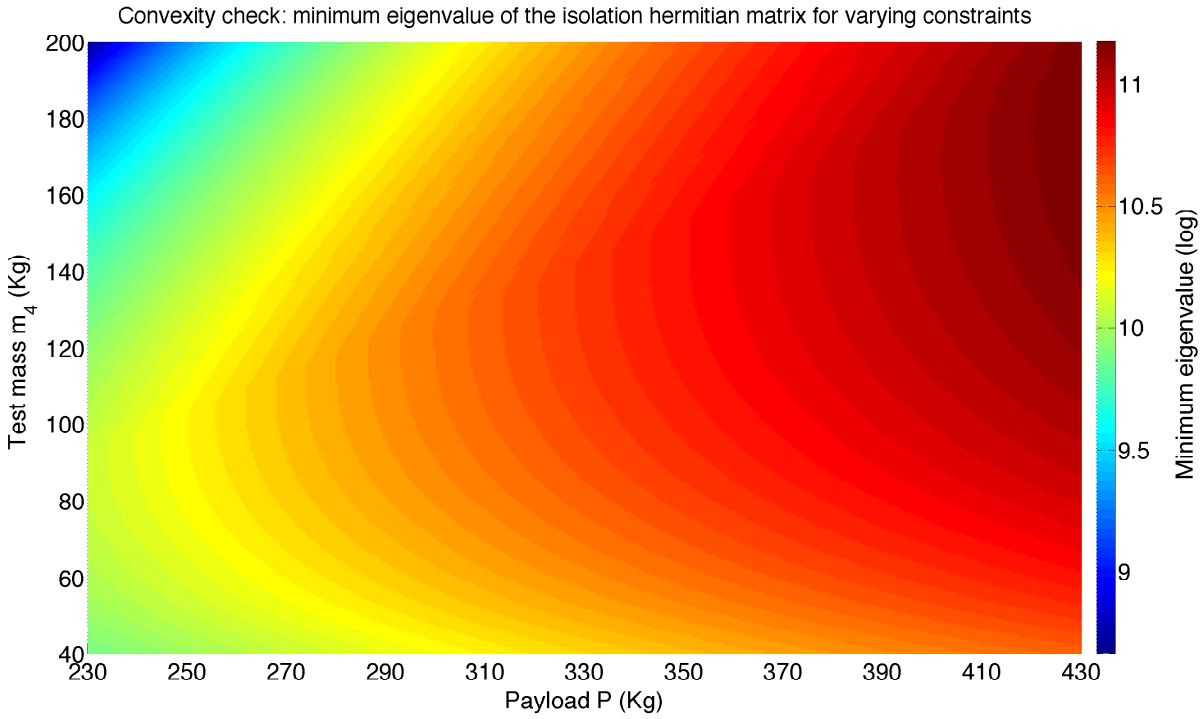

Figure 14: Scanning the LIGO III quad model with the P and m_4 values. The color axis is the log of the smallest eigenvalue at each point in the parameter space. At each point the smallest eigenvalue is the smallest in the entire m_2 and m_3 parameter space (constrained so the no mass is ever less than 10 kg). In other words, Fig. 13 is generated at each point and the smallest value in that figure is what is plotted here. All eigenvalues are greater than zero in the shown range, indicating that the minimization of longitudinal isolation over m_2 and m_3 is convex within what is assumed reasonable bounds for any choice of payload and test mass.

B Bounce Mode Derivation

This section derives Eq. (5), which estimates the vertical bounce mode between the PUM and the test mass, for the case where no springs exist at the PUM. Figure 15 illustrates the conceptual mass spring system used by this estimation. Only the lower half of the quadruple pendulum is considered. Assuming the bounce mode is significantly higher in frequency (at least twice) than all the other vertical modes, this is a valid simplification to make. This simplification is also powerful in that we do not need to know the masses or stiffnesses of the other stages.

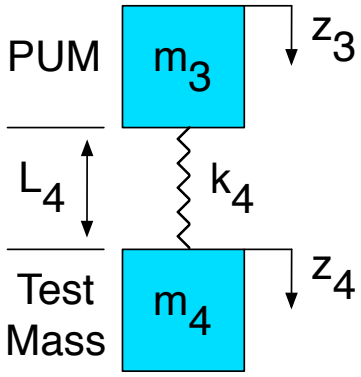

Figure 15: Mass spring system for estimating the bounce frequency between the PUM and test mass.

This system follows the following equation of motion

$$\mathbf{M}\ddot{\mathbf{z}} + \mathbf{K}\mathbf{z} = \mathbf{0}_{2\times 1} \tag{64}$$

where,

$$\mathbf{M} = \begin{bmatrix} m_3 & 0 \\ 0 & m_4 \end{bmatrix} \tag{65}$$

$$\mathbf{K} = \begin{bmatrix} k_4 & -k_4 \\ -k_4 & k_4 \end{bmatrix} \tag{66}$$

$$\mathbf{z} = \begin{bmatrix} z_3 \\ z_4 \end{bmatrix} \tag{67}$$

The mode frequencies are determined by the eigenvalues of this system. The eigenvalues are given by the matrix $\mathbf{M}^{-1}\mathbf{K}$.

$$\mathbf{M}^{-1}\mathbf{K} = \begin{bmatrix} k_4/m_3 & -k_4/m_3 \\ -k_4/m_4 & k_4/m_4 \end{bmatrix} \tag{68}$$

The eigenvalues λ for this matrix are determined by the equation

$$(k_4/m_3 - \lambda)(k_4/m_4 - \lambda) - \frac{k_4^2}{m_3 m_4} = 0 \tag{69}$$

One solution for λ is zero, because the system is free floating. The other is,

$$\lambda = \frac{k_4}{m_3} + \frac{k_4}{m_4} \tag{70}$$

The bounce mode frequency, in rad/s is the square root of λ. Thus, the frequency in Hz is

$$f_{bounce} = \frac{1}{2\pi}\sqrt{\frac{k_4}{m_3} + \frac{k_4}{m_4}} \tag{71}$$

k_4 is given by the cross-sectional area A_4, length L_4, and modulus of elasticity E_4 of the fiber. A factor of 4 is included because we have 4 fibers.

$$k_4 = \frac{4E_4A_4}{L_4} \tag{72}$$

The smallest cross section gives the lowest stiffness and lowest frequency. The smallest cross section is limited by the test mass weight $m_4 g$ and maximum allowed fiber stress σ_4.

$$A_4 = \frac{m_4 g}{4\sigma_4} \tag{73}$$

The factor of 4 is because each fiber carries 1/4 of the load. Thus,

$$k_4 = \frac{E_4 m_4 g}{L_4 \sigma_4} \tag{74}$$

Plugging into the f_{bounce} equation, we reproduce Eq. (5),

$$\boxed{f_{bounce} = \frac{1}{2\pi}\sqrt{\frac{E_4 g}{L_4\sigma_4}\left(1 + \frac{m_4}{m_3}\right)}} \tag{75}$$

References

[1] Madeleine Waller, G1200828-v6, Proposed new pendulum suspension for beyond advanced LIGO 27 August 2012, https://dcc.ligo.org/LIGO-G1200828

[2] Email conversation with Norna Robertson, Maximum Allowed Quadruple Pendulum Weight, 5 March 2013

[3] R. Adhikari, K. Arai, S. Ballmer, E. Gustafson, S. Hild, T1200031-v3, Report of the 3rd Generation LIGO Detector Strawman Workshop, 15 May 2012, https://dcc.ligo.org/LIGO-T1200031

[4] David C. Lay, Linear Algebra and its Applications, 3rd Ed. Addison Wesley 2003

[5] Advanced LIGO Quadruple Pendulum MATLAB Production Model. SVN directory:
/ligo/svncommon/SusSVN/sus/trunk/QUAD/Common/MatlabTools/QuadModel_Production
Make file: ssmake4pv2eMB5f_fiber.m
Parameter file: quadopt_fiber.m

[6] U. Gysin, S. Rast, P. Ruff, E. Meyer, D. W. Lee, P. Vettiger, C. Gerber Temperature dependence of the force sensitivity of silicon cantilevers, 2004, Physical Review B, Volume 69, Number 4, http://prb.aps.org/abstract/PRB/v69/i4/e045403